Highly Ordered Titania Nanotube Arrays Synthesized via One-faced and Single-step Anodization

Thanaporn Thumsa-ard, Udom Tipparach, Narongsak Kodtharin, Orathai Thumthan *

Department of Physics, Faculty of Science, Ubon Ratchathani University, Ubon Ratchathani, 34190 Thailand

Received 6 December 2018; Revised 22 April 2019; Accepted 23 April 2019

Abstract

Highly ordered titania (TiO_2) nanotube arrays were synthesized via one-faced and single-step anodization method. Titanium foils were anodized in ethylene glycol based electrolytes containing 0.25 wt% NH_4F, 2 vol% H_2O, and doped with various concentrations of $K_3[Fe(CN)_6]$ at applied voltage of 50 V for 2 h at room temperature. As-anodized samples were annealed at 450 °C for 2 h in order to transform the amorphous titania to nanocrystalline anatase. Highly ordered titania nanotube arrays were obtained after $K_3[Fe(CN)_6]$ of different concentrations was introduced. The surfaces of TiO_2 nanotubes were smoother after increasing concentrations of $K_3[Fe(CN)_6]$ which were confirmed by AFM investigation. The absorption spectra of the samples were extended in range of 200 to 375 nm and slightly increased in band gap energies of titania when $K_3[Fe(CN)_6]$ was doped. Doping with 0.20 wt% $K_3[Fe(CN)_6]$ caused Ti 2p shifted towards lower binding energy due to the reduction of Ti^{4+} to Ti^{3+} and led to improve the electrochemical performance of titania nanotubes. This work suggests an alternative method for fine tuning the size of TiO_2 nanotube arrays that can be used as energy conversion materials such as dye-sensitized solar cells and solar hydrogen production.

KEYWORDS: Titania; Anodization; Nanotubes; $K_3[Fe(CN)_6]$; Titanium dioxide

*Corresponding authors; e-mail: Orathai.th@ubu.ac.th

Introduction

In recent decades, titanium dioxide nanostructures or titania (TiO_2) such as TiO_2 nanorods [1], TiO_2 nanobelts [2], TiO_2 nanowires [3], TiO_2 nanoparticles [4], TiO_2 nanoflowers [5], TiO_2/TiB_2 nanowalls [6], TiO_2 nanopowders [7], TiO_2 nanosheets [8], TiO_2 nanofibers [9], TiO_2 nanoribbons [10], TiO_2 nanospheres [11], TiO_2 nanodots [12], TiO_2 nanocubes [13], TiO_2 nanoclusters [14], TiO_2 nanocones [15], TiO_2 nanotubes [16], etc., have attracted much attention from scientists and engineers in various areas because of their wide applications in environment [17], photocatalytic [18], dye sensitized solar cell [19], air treatment [20], water splitting [21] and others. In general, titanium dioxide (TiO_2) has three phases including anatase, rutile and brookite. Anatase phase is exceptional in photocatalytic activity due to its high reflective index, low extinction coefficient, non-toxicity, high chemical and physical stabilities and low cost [22]. There are a number of methods to fabricate TiO_2 nanostructures such as hydrothermal synthesis [23], chemical vapor deposition [24], atmospheric pressure plasma jet [25], electrospinning [26], atomic layer deposition [27], and others. Among these, anodization process of TiO_2 nanotubes is the simple and inexpensive. Numerous experimental evidences suggest that TiO_2 nanotubes possess the exceptional properties: high electron transport, large electron diffusion length, and relative band-edge position which are suitable to trigger a wide range of photocatalytic reaction [28, 29]. However, TiO_2 performance is relatively low for the applications of photocatalysis due to its wide band gap energy of 3.0 – 3.2 eV. In order to enhance the performance of TiO_2, it must be improved by doping some elements, for example, Mg and Mg-Nb in TiO_2 [30], Cu on two-dimensional TiO_2 nanowalls [31], S on TiO_2 nanofibers [32], Fe, Ni, Co or Zn on TiO_2 nanoparticles [33], Na on TiO_2 nanorods [34] and CdTe on TiO_2 nanoarchitectures [35]. Previous research has been conducted to improve the performance of TiO_2. For example, the transition-metal-doped TiO_2 nanotubes are highly visible-

active and stable, excellent photoelectrochemical properties, and photocatalytic activities under visible light irradiation [36, 37]. Further, The Fe^{3+} doped TiO_2 nanotubes synthesized by a solvothermal method in $FeCl_3$ solution indicate significant enhancement of the visible light absorption and exhibit excellent photocurrent and photoelectrochemical performance [38].

Here, this study contributes to the enhancement of TiO_2 nanotubes in dye-sensitized solar cell applications and presents the investigation of the effect of potassium ferricyanide ($K_3[Fe(CN)_6]$) on TiO_2 nanotubes. In photoelectrochemical solar cell applications, $K_3[Fe(CN)_6]$ is widely used as photoelectroactive electrolyte [39], because it comprises K, Fe, C, and N which have high potential for improvement on the performance of TiO_2 nanotubes.

In this work, highly ordered TiO_2 nanotubes were fabricated through one-faced and single-step electrochemical anodization on titanium foils by varying amounts of $K_3[Fe(CN)_6]$ in ethylene glycol based electrolyte. The physical and chemical characteristics of as-prepared samples were investigated using X-ray diffraction (XRD), scanning electron microscopy (SEM), atomic force microscopy (AFM), X-ray photoelectron spectroscopy (XPS), and UV-Vis spectroscopy.

Materials and Methods

Preparation of TiO_2 nanotubes and $K_3[Fe(CN)_6]$ doped TiO_2 nanotubes

The 0.25 mm thick titanium foils (99.7% purity) and all chemicals were analytic grade, purchased from Sigma Aldrich. Prior to anodization, the titanium foils were cleaned in a solution containing deionized water and ethanol by ultrasonic cleaner for 40 min and then dried under a flowing air stream. Anodic growth experiments were performed by potentiostatic anodization in a conventional two-electrode compartment electrochemical cell. Then, the pretreated Ti sheet was used as a working electrode (anode) and platinum sheet was used as a counter electrode (cathode). The anodization was performed in ethylene glycol based electrolyte consisting of 0.25 wt% NH_4F and 2 vol% H_2O at applied voltage of 50 V for 2 h at ambient temperature. The separation between the electrodes was 2 cm which made electric field of 2,500 V m^{-1}.

The titania nanotube samples were doped by potassium ferricyanide ($K_3[Fe(CN)_6]$, 99.0% purity) via anodization process. Anodization was conducted in an ethylene glycol solutions consisting of 0.25 wt% NH_4F and 2 vol% H_2O, which were kept constant while the concentrations of $K_3[Fe(CN)_6]$ were varied from 0.05 wt% to 0.20 wt% with increment of 0.05 wt% at applied voltage of 50 V for 2 h at ambient temperature. After anodization, the as-anodized samples were cleaned immediately with pure water using ultrasonic cleaner and then dried in the air stream. The as-anodized samples were annealed at 450 °C for 2 h to transform the amorphous titania to nanocrystalline anatase.

Characterizations of the samples

The crystal structure of the samples was analyzed using X-ray diffraction (XRD). The surface morphology of un-doped and doped TiO_2 nanotube samples were examined using scanning electron microscopy (SEM) and the surface roughness parameter values of all samples were carried out by means of atomic force microscopy (AFM). UV-Vis diffuse reflectance spectra of the samples were recorded using UV-Vis spectroscopy. Elemental analysis of titania nanotube arrays determined by using X-ray photoelectron spectroscopy (XPS).

Results and Discussion

The pore formation of TiO_2 nanotubes can be explained by as follows. After anodization process, oxide films were created over Ti surface due to the interaction of the Ti metal with O^{2-} or OH^- ions and formed initial oxide layers which can be described as follows:

$$2H_2O \rightarrow O_2 + 4e^- + 4H^+ \quad (1)$$

$$Ti + O_2 \rightarrow TiO_2 \quad (2)$$

The oxide layer was etched by NH_4F solution. Under application of an electric field, metal ions of Ti^{4+} migrated from the metal/oxide interface and moved towards the oxide/electrolyte interface. The reaction can be written as follows:

$$TiO_2 + 6F^- + 4H^+ \rightarrow TiF_6^{2-} + 2H_2O \quad (3)$$

After that, the pores of TiO_2 spread uniformly over the surface thus the formation of TiO_2 nanotubes was created [37].

XRD Diffraction patterns

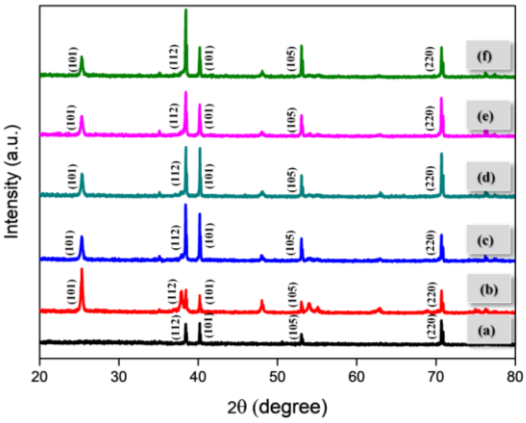

Fig. 1 XRD patterns of TiO_2 nanotube arrays: (a) as-anodized Ti, (b) annealed TiO_2, (c) annealed 0.05 wt% $K_3[Fe(CN)_6]$-doped TiO_2, (d) annealed 0.10 wt% $K_3[Fe(CN)_6]$-doped TiO_2, (e) annealed 0.15 wt% $K_3[Fe(CN)_6]$-doped TiO_2, and (f) annealed 0.20 wt% $K_3[Fe(CN)_6]$-doped TiO_2.

Fig. 1 shows the XRD patterns of TiO_2 nanotube arrays: as-anodized Ti (a), annealed TiO_2 (b) and annealed TiO_2 doped with $K_3[Fe(CN)_6]$ at various concentrations (c, d, e, f). It was observed that as-anodized Ti before calcination appeared peaks belong to Ti metal as shown in line (a). For example, four peaks are located at 2θ = 38.0°, 40.0°, 57.5°, and 71.0° corresponding to Ti (112), (101), (105), and (220) planes with the interplanar spacings (d) of 0.06, 0.11, 0.07, and 0.03 nm, respectively, derived by hexagonal crystal structure of Ti metal [40]. This XRD pattern indicated that as-anodized sample was amorphous layer on top of Ti metal sheet. In other word, anatase phase structure of as-anodized Ti (a) was not observed. In contrast, after as-anodized TiO_2 (b) and the TiO_2 were doped with $K_3[Fe(CN)_6]$ were annealed at 450 °C for 2 h, the XRD peaks suggested that phase transformation from amorphous phase to anatase phase occurred. Four peaks located at 2θ = 25.5°, 38.0°, 57.5°, and 71.0 ° corresponding to the anatase (101), (112), (105), and (220) planes with the interplanar spacing (d) of 0.35, 0.23, 0.17, and 0.13 nm, respectively. These data were derived by tetragonal crystal structure of TiO_2 that was suitable for the applications in dye-sensitized solar cells [41]. For $K_3[Fe(CN)_6]$ doped titania nanotube samples, the phase of dopants was undetectable by XRD even for highly $K_3[Fe(CN)_6]$ doped samples.

SEM images

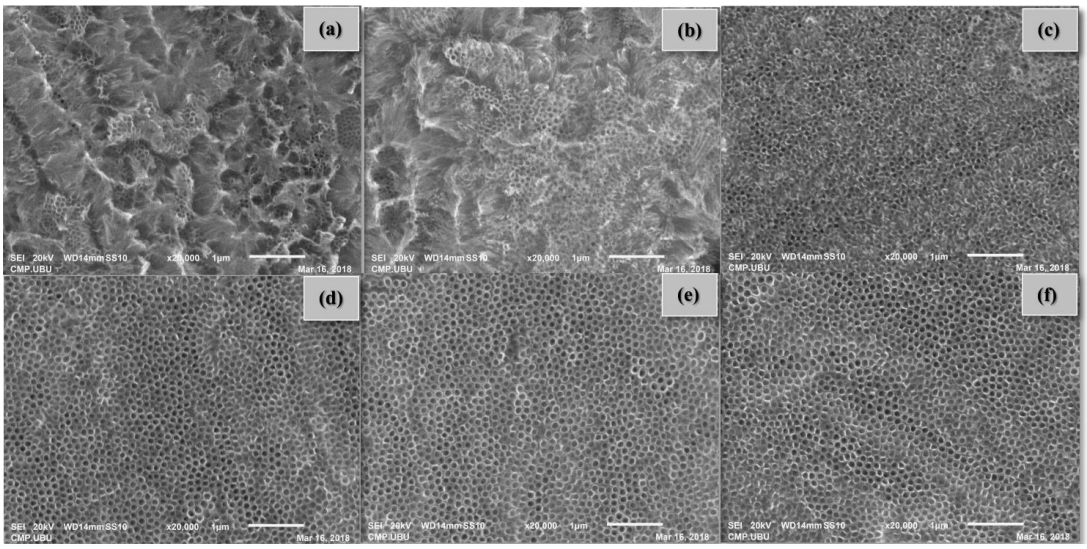

Fig. 2 SEM images of TiO_2 nanotube arrays: (a) as-anodized Ti, (b) annealed TiO_2, (c) annealed 0.05 wt% $K_3[Fe(CN)_6]$-doped TiO_2, (d) annealed 0.10 wt% $K_3[Fe(CN)_6]$-doped TiO_2, (e) annealed 0.15 wt% $K_3[Fe(CN)_6]$-doped TiO_2, and (f) annealed 0.20 wt% $K_3[Fe(CN)_6]$-doped TiO_2.

The detailed surface morphological characterization of as-prepared samples was examined by scanning electron microscopy (SEM) as compared in Fig. 2. The SEM investigation reveals that the amorphous nanotube region of as-anodized Ti (a) before annealing was not homogenous and appeared less number of nanotubes than pure TiO_2 sample (b) and

$K_3[Fe(CN)_6]$ doped TiO_2 nanotube samples (c, d, e, f) after annealing. The diameters of titania nanotube samples were approximately 90 nm, 100 nm, 140 nm, 120 nm, 105 nm, and 120 nm for (a) as-anodized Ti, (b) annealed TiO_2, (c) annealed 0.05 wt% $K_3[Fe(CN)_6]$-doped TiO_2, (d) annealed 0.10 wt% $K_3[Fe(CN)_6]$ doped-TiO_2, (e) annealed 0.15 wt% $K_3[Fe(CN)_6]$-doped TiO_2, and (f) annealed 0.20 wt% $K_3[Fe(CN)_6]$-doped TiO_2, respectively.

Interestingly, the highly ordered nanotube arrangements were found after as-anodized TiO_2 nanotubes were doped with increasing concentrations of $K_3[Fe(CN)_6]$. The effect of the concentration of $K_3[Fe(CN)_6]$ on TiO_2 nanotube arrangement can be described as follows. During the pore formation process, if the formation and dissolution of oxide layer are in an optimum range, highly self-organized oxide pore arrangement or nanotube formation is possible. It is noteworthy that the formation of reaction products also increases the conductivity of the electrolyte and thereby increases the growth rate of the nanotubes [40]. The rate of electron transfer for the ferrocyanide couple on platinum electrodes increases linearly with increasing concentration of added cation. Ferrocyanide solution acts as a buffer during respective formation of the mono, di, tri, and tetra protonated ferricyanide electrolyte [38]. Besides, $K_3[Fe(CN)_6]$ as a buffer solution in the electrolyte can also create the pH gradient which is required for fabricating the nanotubes with longer length. However, increasing the $K_3[Fe(CN)_6]$ concentration in the electrolyte is effective on the pH gradient and yields to the enhancement of the growth rate of nanotubes, respectively [43, 44].

UV-visible spectra analysis

Optical properties of samples were effectively characterized using UV-visible spectroscopy. The UV-visible absorption spectra of as-anodized Ti sample before annealing (a), pure anodized TiO_2 nanotube sample (b), and various concentrations of $K_3[Fe(CN)_6]$ doped anodized TiO_2 nanotube samples after annealing at 450 °C for 2 h (c, d, e, f) were measured and shown in Fig. 3. The optical band gap energy of all titania nanotube samples were calculated using a Tauc plot of the modified Kubelka-Munk (MK) function with a linear extrapolation [45 – 48] as given below.

$$(\alpha h\upsilon)^{1/2} = \beta(h\upsilon - E_g) \quad (4)$$

where, E_g is the Tauc optical band gap, α = 2.303A/d (A is optical intensity, and d is thickness of the sample), ν is the frequency of incident light, β is a constant which depends on the width of the localized states in the band gap and h is Planck's constant.

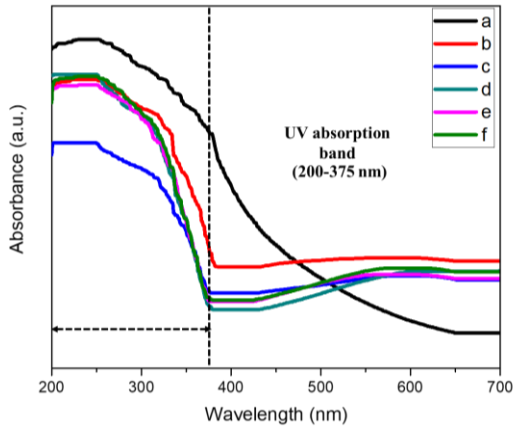

Fig. 3 Absorbance UV-visible spectra of TiO_2 nanotube arrays: (a) as-anodized Ti, (b) annealed TiO_2, (c) annealed 0.05 wt% $K_3[Fe(CN)_6]$-doped TiO_2, (d) annealed 0.10 wt% $K_3[Fe(CN)_6]$-doped TiO_2, (e) annealed 0.15 wt% $K_3[Fe(CN)_6]$-doped TiO_2, and (f) annealed 0.20 wt% $K_3[Fe(CN)_6]$-doped TiO_2.

To further investigate the effect of $K_3[Fe(CN)_6]$ dopant on the optical response of TiO_2 nanotube arrays, UV-Vis spectroscopy of the titania nanotube samples were measured. The absorbance spectra of all obtained samples are demonstrated in Fig. 3. As expected, an intense UV absorption band appeared in rang of 200 to 375 nm in all titania nanotube samples, corresponding to electron-transition from a valence band to a conduction band.

The comparison of $(\alpha h\upsilon)^{1/2}$ vs. $h\upsilon$ plots are displayed in Fig. 4 to estimated band gap energy of (a) as-anodized Ti, (b) annealed TiO_2, (c) annealed 0.05 wt% $K_3[Fe(CN)_6]$-doped TiO_2, (d) annealed 0.10 wt% $K_3[Fe(CN)_6]$-doped TiO_2, (e) annealed 0.15 wt% $K_3[Fe(CN)_6]$-doped TiO_2, and (f) annealed 0.20 wt% $K_3[Fe(CN)_6]$-doped TiO_2. It was found that band gap energy of as-anodized Ti after annealing at 450 °C for 2 h increased from 1.7 eV to 2.3 eV. Moreover, incorporation of $K_3[Fe(CN)_6]$ into TiO_2 nanotubes had effect on band gap energy of TiO_2 nanotube samples that slightly increased from 2.3 eV to 2.9 eV with increasing concentrations of $K_3[Fe(CN)_6]$.

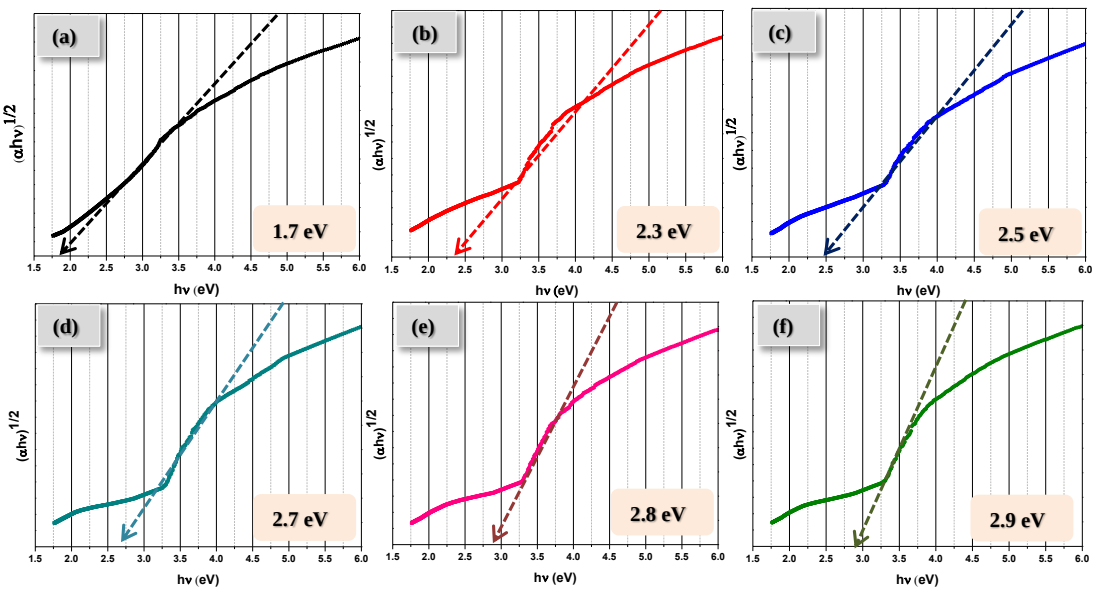

Fig. 4 Plot of $(\alpha h\upsilon)^{1/2}$ vs. $h\upsilon$ employed to calculate the band gap value of TiO_2 nanotube arrays: (a) as-anodized Ti, (b) annealed TiO_2, (c) annealed 0.05 wt% $K_3[Fe(CN)_6]$-doped TiO_2, (d) annealed 0.10 wt% $K_3[Fe(CN)_6]$-doped TiO_2, (e) annealed 0.15 wt% $K_3[Fe(CN)_6]$-doped TiO_2, and (f) annealed 0.20 wt% $K_3[Fe(CN)_6]$-doped TiO_2.

According to Goldschmidt-Pauling rule, by increasing the concentration of transition metal as a dopant can cause an increase in band gap energy. The band gap energy between the valence band and the conduction depends uniquely on the first Fourier coefficient of the crystal potential changes insignificantly with solid size. Therefore, a perturbation to the crystal potential can cause band gap energy to be changed. The ionic radius of Fe^{3+} (0.78 Å) is larger than that of Ti^{4+} (0·74 Å). This result in the bond length of Fe-Ti and Fe-O becomes smaller; in other words, the bond of Fe-Ti and Fe-O contracted. Due to the Goldschmidt-Pauling rule of bond contraction induced by under coordination [49], this result may increase of band gap of titania nanotubes after introducing potassium ferricyanide. Moreover, the increase of band gap is observed as the tube diameter increases [50]. The band gap energy of TiO_2 nanotube samples, after introduced $K_3[Fe(CN)_6]$ with various concentrations, increased from 2.3 eV to 2.5, 2.7, 2.8, and 2.9 eV. In addition, crystallite size of TiO_2 changed from 100 nm to 140, 120, 105, and 120 nm for 0.05 wt%, 0.10 wt%, 0.15 wt%, and 0.20 wt% of $K_3[Fe(CN)_6]$, respectively.

AFM analysis

The surface morphology of the titania nanotube samples was studied by means of Atomic force microscopy (AFM). Two-and three-dimensional AFM images of TiO_2 nanotubes (a) as-anodized Ti before annealing, (b) annealed TiO_2, (c) annealed 0.05 wt% $K_3[Fe(CN)_6]$-doped TiO_2, (d) annealed 0.10 wt% $K_3[Fe(CN)_6]$-doped TiO_2, (e) annealed 0.15wt% $K_3[Fe(CN)_6]$-doped TiO_2, and (f) annealed 0.20 wt% $K_3[Fe(CN)_6]$-doped TiO_2 after annealing at 450 °C for 2 hours are shown in Fig. 5.

From AFM data analysis, different conditions of anodization yielded different surface morphology of roughness. Table 1 shows three surface roughness parameters: the root mean square roughness (R_q), ratio of peak to valley (R_{p-v}), and average roughness (R_{ave}) [51] of the samples. It is significant to notice that the average roughness can be the same for two surfaces, while their roughness profiles were completely different. The three parameters of titania nanotube samples generally decreased by increasing concentrations of $K_3[Fe(CN)_6]$ after annealing. The reduction of ratio of peak to valley (R_{p-v}) after doping of $K_3[Fe(CN)_6]$ on titania nanotube samples means that the surface were smoother. This may give initial evidence that there was the reduction in the surface to volume ratio after introducing $K_3[Fe(CN)_6]$ into titania nanotubes.

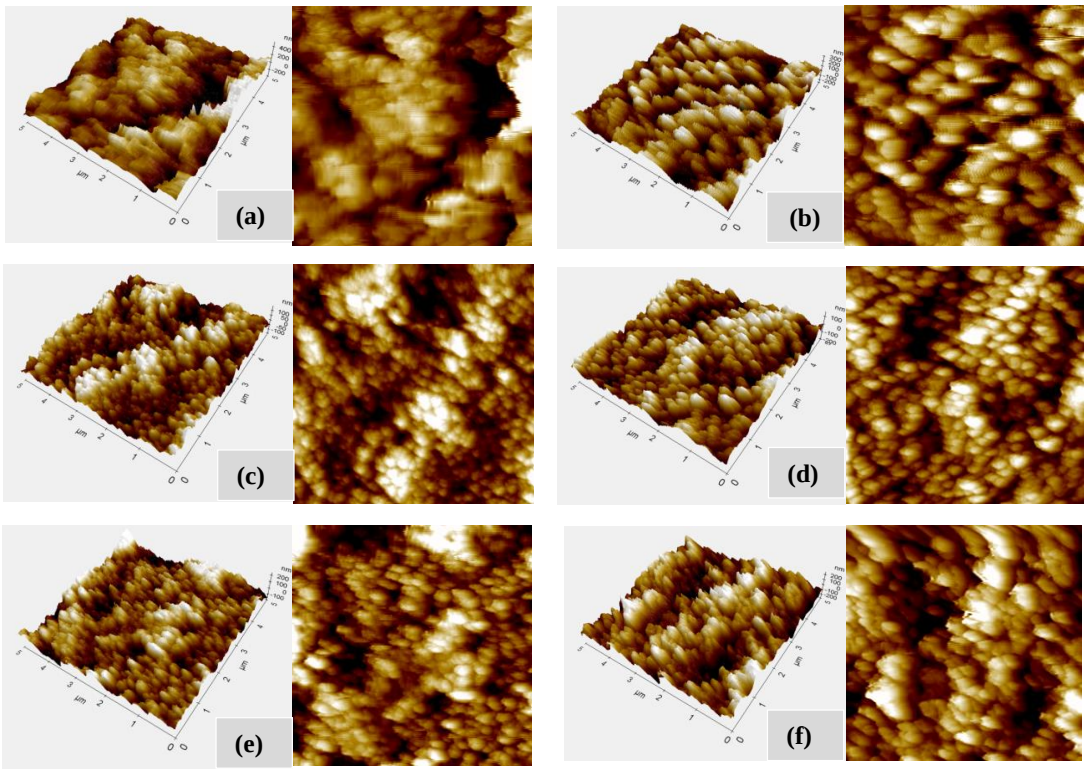

Fig. 5 Two-and three-dimensional AFM images of TiO_2 nanotube arrays: (a) as-anodized Ti, (b) annealed TiO_2, (c) annealed 0.05 wt% $K_3[Fe(CN)_6]$-doped TiO_2, (d) annealed 0.10 wt% $K_3[Fe(CN)_6]$-doped TiO_2, (e) annealed 0.15 wt% $K_3[Fe(CN)_6]$-doped TiO_2, and (f) annealed 0.20 wt% $K_3[Fe(CN)_6]$-doped TiO_2.

Table 1 Surface roughness parameters values from AFM measurement for titania nanotube samples.

Samples	R_{p-v} (nm)	R_q (nm)	R_{ave} (nm)
As-anodized Ti (a)	903.661	97.960	74.942
Annealed TiO_2 (b)	575.238	71.130	56.866
Annealed 0.05 $K_3[Fe(CN)_6]$ doped TiO_2 (c)	434.774	48.093	38.001
Annealed 0.10 $K_3[Fe(CN)_6]$ doped TiO_2 (d)	361.202	48.289	37.715
Annealed 0.15 $K_3[Fe(CN)_6]$ doped TiO_2 (e)	290.625	46.389	37.413
Annealed 0.20 $K_3[Fe(CN)_6]$ doped TiO_2.(f)	276.383	41.139	33.271

XPS analysis

The chemical states of the prepared samples were characterized using XPS as shown in Fig. 6. Overall XPS spectra of all prepared samples appeared peaks of Ti 2p, O 1s, and C 1s while the peaks of Fe and N were not observed in the XPS spectra for $K_3[Fe(CN)_6]$ doped titania nanotube samples. Two peaks of Ti 2p XPS spectra of all prepared samples were observed. Ti $2p_{3/2}$ at approximately 458.64 eV and Ti $2p_{1/2}$ at approximately 464.35 eV were assigned to the Ti-O metal oxide bonding [52, 53]. The distance between them was approximately 5.71 eV which confirmed that the main chemical state of Ti inTiO_2 nanotube lattices is Ti^{4+} [54].

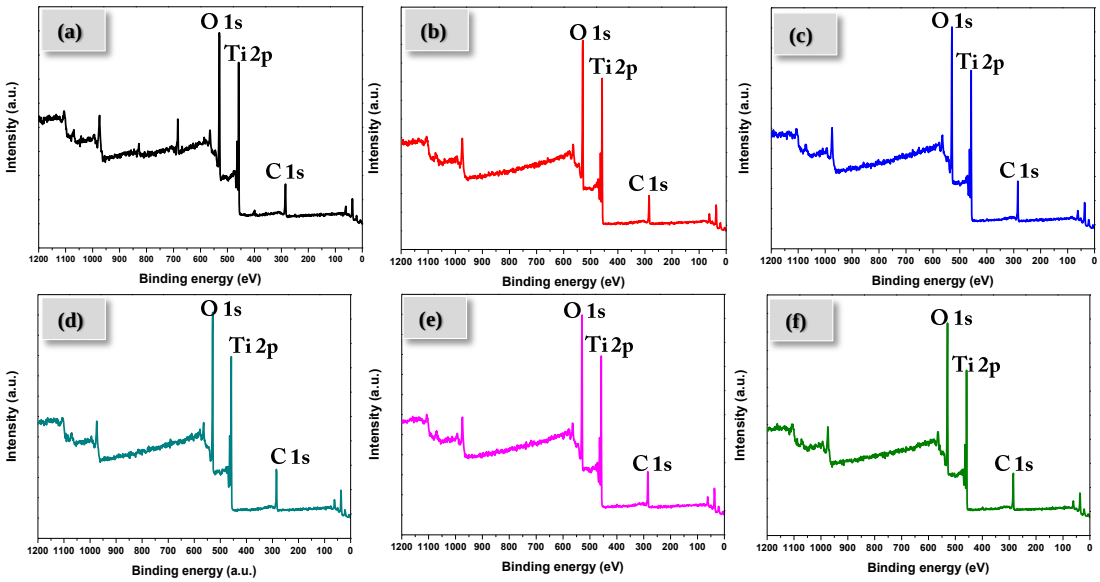

Fig. 6 Over all XPS spectra of TiO_2 nanotube arrays: (a) as-anodized Ti, (b) annealed TiO_2, (c) annealed 0.05 wt% $K_3[Fe(CN)_6]$-doped TiO_2, (d) annealed 0.10 wt% $K_3[Fe(CN)_6]$- doped TiO_2, (e) annealed 0.15 wt% $K_3[Fe(CN)_6]$-doped TiO_2, and (f) annealed 0.20 wt% $K_3[Fe(CN)_6]$-doped TiO_2.

Moreover, it was found that the introduction of $K_3[Fe(CN)_6]$ at concentration of 0.20 wt% had effect on binding energy of Ti 2p that shifted towards lower binding energy from 458.64 eV and 464.35 eV to 457.69 eV and 463.39 eV for Ti $2p_{3/2}$ and Ti $2p_{1/2}$, respectively as compared in Fig. 7.

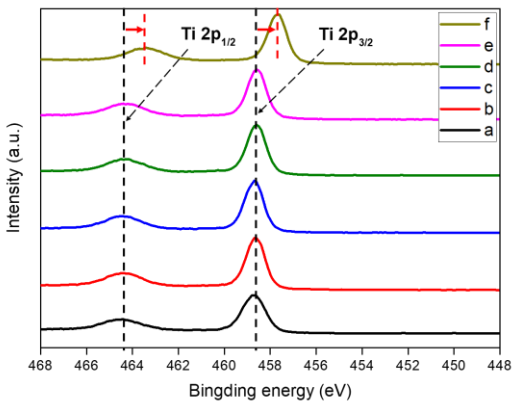

Fig. 7 The comparison of Ti 2p line shapes of TiO_2 nanotube arrays: (a) as-anodized Ti, (b) annealed TiO_2, (c) annealed 0.05 wt% $K_3[Fe(CN)_6]$-doped TiO_2, (d) annealed 0.10 wt% $K_3[Fe(CN)_6]$-doped TiO_2, (e) annealed 0.15 wt% $K_3[Fe(CN)_6]$-doped TiO_2, and (f) annealed 0.20 wt% $K_3[Fe(CN)_6]$-doped TiO_2.

The energy shift occurred to all titania nanotube samples which suggested that this could be a result of reduction of Ti^{4+} to Ti^{3+}. Accordingly, the negative charge introduced in the lattice of nanotubes is compensated by conversion of Ti^{4+} to Ti^{3+}.This conversion utilized the charge transfer between anions and cations due to the higher percentage of loosely bound Ti^{3+}-O bonds compared with the stronger Ti^{4+}-O bonds. Consequently, the electrochemical performance of titania nanotubes was enhanced. Further, this less oxidized Ti^{3+} states indicated higher oxygen deficiencies within the titania nanotubes [55, 56]. The O 1s XPS spectra of all samples at approximately 529.87 eV was assigned to the O - Ti bonding [57]. The C 1s XPS spectra of all prepared samples at approximately 284.9 eV was assigned, due to carbon absorption on the surface as pollutant (C-C bonds) [58].

Conclusion

This work reports the effect of $K_3[Fe(CN)_6]$ on the performance of TiO_2 nanotubes. Highly ordered TiO_2 nanotubes were successfully fabricated via one-faced and single-step anodizing technique. XRD analysis confirmed that TiO_2 nanotubes was crystalline and exhibited anatase phase for all samples after annealing at 450 °C for 2 h. Interestingly, the highly order nanotube arrays were found after $K_3[Fe(CN)_6]$ at

various concentration was doped. The three surface roughness parameter values from AFM measurement of TiO_2 nanotubes decreased with increasing concentrations of $K_3[Fe(CN)_6]$, which made the surface of TiO_2 nanotubes were smoother. UV-visible absorbance spectra demonstrated that doping of $K_3[Fe(CN)_6]$ successfully extended the absorption spectrum of all titania nanotube samples in range of 200 to 375 nm and slightly increased their band gap energy. XPS data revealed that all titania nanotube samples composed of Ti and O. Although Fe and N were not detected in XPS measurement, doping of $K_3[Fe(CN)_6]$ at concentration of 0.20 wt% caused Ti 2p shifted towards lower binding energy. This could be a result of reduction of Ti^{4+} to Ti^{3+}, thus improving the photocatalytic reaction of titania nanotubes. This fabricated 0.20 wt% of $K_3[Fe(CN)_6]$ doped TiO_2 nanotubes are potential candidate to be used as energy conversion materials

Acknowledgements

One of the authors, Thanaporn Thumsa-ard, gratefully acknowledges the financial support for this work from Science Achievement Scholarship of Thailand. We thank the Department of Physics, Faculty of Science, Ubon Ratchathani University for providing research grants and facilities.

References

[1] T. Plirdpring, B. Samransuksamer, M. Horprathum, T. Lertvanithpol, V. Pattantsetakul, S. Limwichean, N. Nuntawong, T. Boonpichayapha, P. Eiamchai, Preparation and surface wettability of nanostructure TiO_2 films, Mater. Today.: Proc. 4 (2017) 6331 – 6335.

[2] Q. Chen, H. Liu, Y. Xin, X. Cheng, TiO_2 nanobelts-Effect of calcination temperature on optical, photoelectrochemical and photocatalytic properties, Electrochim. Acta. 111 (2013) 284 – 291.

[3] J. Du, X. Gu, H. Guo, J. Liu, Q. Wu, J. Zou, Self-induced preparation of TiO_2 nanowires by chemical vapor deposition, J. Cryst. Growth. 427 (2015) 54 – 59.

[4] M.M. Viana, V.F. Soares, N.D.S. Mohallem, Synthesis and characterization of TiO_2 nanoparticles, Ceram. Int. 36 (2010) 204 – 2053.

[5] J. Ma, W. Ren, J. Zhao, H. Yang, Growth of TiO_2 nanoflowers photoanode for dye-sensitized solar cells, J. Alloys Compd. 692 (2017) 1004 – 1009.

[6] F. Huang, A. Yan, Z. Fu, S. Yin, F. Zhang, Y. Qiang, Self-assembled synthesis of TiO_2/TiB_2 nanowall and its photocatalytic properties, J. Alloys Compd. 574 (2013) 49 – 53.

[7] S.M. Oh, T. Ishigaki, Preparation of pure rutile and anatase TiO_2 nanopowders using RF thermal plasma, Thin Solid Films, 457 (2004) 186 –191.

[8] R. Edy, Y. Zhao, G.S. Huang, J.J. Shi, J. Zhang, A.A. Solovev, Y. Mei, TiO_2 nanosheets synthesized by atomic layer deposition for photocatalysis, Prog. Nat. Sci.: Mat. Int. 26 (2016) 493 – 497.

[9] M. Vahtrus, A. Šutka, S. Vlassov, A. Šutka, B. Polyakov, R. Saar, L. Dorogin, R. Lõhmus, Mechanical characterization of TiO_2 nanofibers produced by different electrospinning techniques, Mater. Charact. 100 (2015) 98 – 103.

[10] Q. Yu, M. Wang, H. Chen, Fabrication of ordered TiO_2 nanoribbon arrays by electrospinning, Mater. Lett. 64 (2010) 428 – 430.

[11] M. Kazazi, P. Abdollahi, M.M. Moghadam, High surface area TiO_2 nanospheres as a high-rate anode material for aqueous aluminium-ion batteries, Solid State Ionics. 300 (2017) 32 – 37.

[12] G. Cheng, F.J. Stadler, Facile synthesis and characterization of TiO_2 nanodots and TiO_2 nanodots@MWCNTs composite via solvothermal method, Mater. Lett. 113 (2013) 71 – 75.

[13] Y. Zhou, E.Y. Ding, W.D. Liab, Synthesis of TiO_2 nanocubes induced by cellulose nanocrystal (CNC) at low temperature, Mater. Lett. 61 (2007) 5050 – 5052.

[14] K.T. Park, V. Meunier, M.H. Pan, W.A. Shelton, N.H. Yu, E.W. Plummer, Nanoclusters of TiO_2 wetted with gold, Surf. Sci. 603 (2009) 3131 – 3135.

[15] D. Zhong, B. Cai, X. Wang, Z. Yang, Y. Xing, S. Miao, W.H. Zhang, C. Lia, Synthesis of oriented TiO_2 nanocones with fast charge transfer for perovskite solar cells, Nano Energy. 11 (2015) 409 – 418.

[16] C.B.D. Marien, T. Cottineau, D. Robert, P. Drogui, TiO_2 Nanotube arrays: Influence of tube length on the photocatalytic degradation of Paraquat, Appl. Catal., B. 194 (2016) 1 – 6.

[17] B. Sarkar, N. Singhal, R. Goyal, A. Bordoloi, L.N. Sivakumar ,K.U. Kumar, R. Bal, Morphology-controlled synthesis of TiO_2 nanostructures for environmental application, Catal. Commun. 74 (2016) 43 – 48.

[18] A. Pal, T.K. Jana, K. Chatterjee, Silica supported TiO_2 nanostructures for highly efficient photocatalytic application under visible light irradiation, Mater. Res. Bull. 76 (2016) 353 – 357.

[19] M. Bhogaita, S. Yadav, A.U. Bhanushali, A.A. Parsola, R.P. Nalini, Synthesis characterization of TiO_2 thin films for DSSC prototype, Mater. Today: Proc. 3 (2016) 2052 – 2061.

[20] M.D. Hernández-Alonso, S. García-Rodríguez, S. Suárez, R. Portela, B. Sánchez, J.M. Coronado, Highly selective one-dimensional TiO_2-based nanostructures for air treatment applications, Appl. Catal., B. 110 (2011) 251 – 259.

[21] T.S. Atabaev, M.A. Hossain, D. Lee, H.K. ook Kim, Y.H. Hwang, Pt-coated TiO_2 nanorods for photoelectrochemical water splitting applications, Results Phys. 6 (2016) 373 – 376.

[22] S. Ananth, T. Arumanayagam, P. Vivek, P. Murugakoothan, Direct synthesis of natural dye mixed titanium dioxide nano particles by sol-gel method for dye sensitized solar cell applications, Optik - Int. J. Light and Electron Optics. 125 (2014) 495 – 498.

[23] S. Zanganehae, A. Kajbafvalab, N. Zanganehc, R. Molaeid, M.R. Bayatid, H.R. Zargard, S.K. Sadrnezhaade, Hydrothermal synthesis and characterization of TiO_2 nanostructures using LiOH as a solvent, Adv. Powder Technol. 22 (2011) 336 – 339.

[24] S.Y. Kim, J.H. Yu, J.S. Lee, The characteristics of nanosized TiO_2 powders synthesized by chemical vapor condensation, Nanostruct. Mater. 12 (1999) 471 – 474.

[25] Z. Liu, Q. Chen, Z. Wang, L. Yang, C. Wang, Production of titanium dioxide powders by atmospheric pressure plasma jet, Physics Procedia. 18 (2011) 168 – 173.

[26] S. Suphankij, W. Mekprasart, W. Pecharapa, Photocatalytic of N-doped TiO_2 Nanofibers Prepared by Electrospinning, Energy Procedia. 34 (2013) 751 – 756.

[27] P. Uudeküll, J. Kozlov, H. Mändar, J. Link, M. Sihtmä, S. Käosaar, I. Blinova, K. Kasemets, A. Kahru, R. Stern, T. Tätte, K. Kukli, A. Tamm, J. Magn, Atomic layer deposition of titanium oxide films on As-synthesized magnetic Ni particles: Magnetic and safety properties, Mater. 429 (2017) 299 – 304.

[28] X. Zhou, N.T. Nguyen, S. Ö. PatrikSchmuki, Anodic TiO_2 nanotube layers: Why does self-organized growth occur-A mini review, Electrochem. Commun. 46 (2014) 157 – 162.

[29] G. CAO, B. CUI ,W. WANG, G. TANG, Y. FEN, G.L. WANG, Fabrication and photodegradation properties of TiO_2 nanotubes on porous Ti by anodization, Transactions of Nonferrous Metals Society of China. 24 (2014) 2581 – 2587.

[30] A. Sasani, A. Baktash, K. Mirabbaszadeh, B. Khoshnevisan, Structural and electronic properties of Mg and Mg-Nb co-doped TiO_2 (101) anatase surface, Appl. Surf. Sci. 384 (2016) 298 – 303.

[31] D. Dahlan, S. Khatijah, M. Saad, A. Usra Berli, A. Bajili, A.A. Umar, Synthesis of two-dimensional nanowall of Cu-Doped TiO_2 and its application as photoanode in DSSCs, Physica E: Low-dimensional Systems and Nanostructures. 91(2017) 185 – 189.

[32] M.S. Mahmoud, M.S. Akhtar, I.M.A. Mohamed, R. Hamdan, Y.A. Dakk, N.A.M. Barakat, Demonstrated photons to electron activity of S-doped TiO_2 nanofibers as photoanode in the DSSC, Mater. Lett. 225 (2018) 77 – 81.

[33] B. Ünlü, S. Çakar, M. Özacar, The effects of metal doped TiO_2 and dithizone-metal complexes on DSSCs performance, Sol. Energy. 166 (2018) 441 – 449.

[34] S. Shalini, N. Prabavathy, R. Balasundaraprabhu, T.S. Kumar, D. Velauthapillai, P. Balraju, S. Prasanna, Studies on DSSC encompassing flower shaped assembly of Na-doped TiO_2 nanorods sensitized with extract from petals of Kigelia Africana, Optik-Int. J. for Light and Electron Optics, 155(2018) 334 – 343.

[35] A.K. Pandey, M.S. Ahmad, M. Alizadeh, N.A. Rahim, Improved electron density through hetero-junction binary sensitized TiO_2/ CdTe / D719 system as photoanode for dye sensitized solar cell, Physica E: Low-dimensional Systems and Nanostructures. 101 (2018) 139 – 143.

[36] M.M. Momeni, Y. Ghayeb, S. Gheibee, Silver nanoparticles decorated titanium dioxide-tungsten trioxide nanotube films with enhanced visible light photo catalytic activity, Ceram. Int. 43 (2017) 564 – 570.

[37] X. Zhou, F. Peng, H. Wang, H. Yu, J. Yang, Preparation of B, N-codoped nanotube arrays and their enhanced visible light photoelectrochemical performances, Electrochem. Commun. 13 (2011) 121 – 124.

[38] Q. Wang, R. Jin, M. Zhang, S. Gao, Solvothermal preparation of Fe-doped TiO_2 nanotube arrays for enhancement in visible light induced photoelectrochemical performance, J. Alloy. Comp. 690 (2017) 139 – 144.

[39] D. Peramunage, S. Licht, Ligand, cation and speciation effects on n-cdSe([KFe(CN)6]3-2-) photoelectrochemistry, Sol. Energy. 52 (1994) 197 – 204.

[40] M.G. Hosseini, M.M. Momeni M. Faraji, Fabrication of Au-Nanoparticle/TiO_2-Nanotubes Electrodes Using Electrochemical Methods and Their Application for Electrocatalytic Oxidation of Hydroquinone, Electroanalysis. 23 (2011) 1654 – 1662.

[41] Y. Marsumi1, A.W. Pramono1, Influence of Niobium or Molybdenum in Titanium Alloy for Permanent Implant Application, Adv. Mater. Res. 900 (2014) 53 – 63.

[42] K. Lee, Anca Mazare, P. Schmuki, One-Dimensional Titanium Dioxide Nanomaterials: Nanotubes, Chem. Rev. 114 (19) 9385 – 9454.

[43] G.K. Mor, O.K. Varghese, M. Paulose, K. Shankar, C.A. Grimes, A review on highly ordered, vertically oriented TiO_2 nanotube arrays: Fabrication, material properties, and solar energy applications, Sol. Energy Mater. Sol. Cells. 90 (2006) 2011 – 2075.

[44] M. Alitabar, H. Yoozbashizadeh, Effect of sodium carbonate as an additive on the morphology and photocatalytic activity of TiO_2 nanotubes, Mater. Res. Bull. 95 (2017) 169 – 176.

[45] S.A. Kazmi, S. Hameed, A.S. Ahmed, M. Arshad, A. Azam, Electrical and optical properties of graphene-TiO_2 nanocomposite and its applications in dye sensitized solar cells (DSSC), J. Alloys Compd. 691 (2017) 659 – 665.

[46] M. Alitabar, H. Yoozbashizadeh, Effect of sodium carbonate as an additive on the morphology and photocatalytic activity of TiO_2 nanotubes, Mater. Res. Bull. 95 (2017) 169 – 176.

[47] A.A. Yadav, E.U. Masumdar, Preparation and characterization of indium doped CdS0.2Se0.8 thin films by spray pyrolysis, Mater. Res. Bull. 45 (2010) 1455 – 1459.

[48] M. MohsenMomeni, Photoelectrochemical water splitting on chromium-doped titanium dioxide nanotube photoanodes prepared by single-step anodizing, J. Alloys Compd. 637 (2015) 393 – 400.

[49] M. Zolfaghari, M. Chireh, Effect of Mn Dopant on Lattice Parameters and Band Gap Energy of Semiconductor ZnO Nanoparticles, Adv. Mater. Res. 829 (2014) 784 – 789.

[50] S. Khajoei Gharaei, M. Abbasnejad, Ryo Maezono, Bandgap reduction of photocatalytic TiO_2 nanotube by Cu doping, Sci. Re. 8 (2018) 1 – 10.

[51] K. Carneiro, C.P. Jensen, J.F. Jørgensen, J. Garnœs, P.A. McKeown, Roughness Parameters of Surfaces by Atomic Force Microscopy, CIRP Annals. 44 (1995) 517 – 522.

[52] D. Tang, Y. Wang, Y. Zhao, Y. Yang, L. Zhang, X. Mao, Effect of the composition of Ti alloy on the photocatalytic activities of Ti-based oxide nanotube arrays prepared by anodic oxidation, Appl. Surf. Sci. 319 (2014) 81 – 188.

[53] G. Hopfengärtner, D. Borgmann, I. Rademacher, G. Wedler, E. Hums, G.W. Spitznagel, XPS studies of oxidic model catalysts: Internal standards and oxidation numbers, J. Electron. Spectrosc. Relat. Phenom. 63 (1993) 91 – 116.

[54] L. Gomathi Devi, R. Kavitha, A review on nonmetal ion doped titania for the photocatalytic degradation of organic pollutants under UV/solar light: Role of photogenerated charge carrier dynamics in enhancing the activity, Appl. Catal., B: Environmental. 140 – 141 (2013) 559 – 587.

[55] V.C. Anitha, A.N. Banerjee, G.R. Dillip, S.W. Joo, B.K. Min, Nonstoichiometry-Induced Enhancement of Electrochemical Capacitance in Anodic TiO_2 Nanotubes with Controlled Pore Diameter, J. Phys. Chem. C. 120 (2016) 9569 – 9580.

[56] L.K. Preethi1, R.P. Antony, T. Mathews1, L. Walczak, C.S. Gopinath, A Study on Doped Heterojunctions in TiO_2 Nanotubes: An Efficient Photocatalyst for Solar Water Splitting, Sci. Rep. 7 (2017) 14314.

[57] C. Hinnen, D. Imbert, J.M. Siffre, P. Marcus, An in situ XPS study of sputter-deposited aluminium thin films on graphite, Appl. Surf. Sci. 78 (1994) 219 – 223.

[58] M. Alitabar, H. Yoozbashizadeh, Improving the visible light photoelectrochemical activity of synthesized TiO_2 nanotube arrays in an organic electrolyte containing sodium carbonate with doping by copper via single-step anodization, N. J. Chem. 41 (2017) 10723 – 10730.